Characteristics of internal solitary waves in the Maluku Sea, Indonesia

Adi Purwandana, Yannis Cuypers

Oceanologia xxx (xxxx) xxx

Available online at www.sciencedirect.com

ScienceDirect

journal homepage: www.journals.elsevier.com/oceanologia

ORIGINAL RESEARCH ARTICLE

Characteristics of internal solitary waves in the Maluku Sea, Indonesia

Adi Purwandana[a,*], **Yannis Cuypers**[b]

[a] *Research Center for Oceanography, National Research and Innovation Agency (RCO-BRIN), Jakarta, Indonesia*
[b] *Laboratory of Oceanography and Climatology via Experimentation and Numerical Approach (LOCEAN), Sorbonne University, Paris, France*

Received 22 February 2022; accepted 26 July 2022
Available online xxx

KEYWORDS
Internal tide;
Internal wave;
Ternate waters;
Lifamatola Passage;
Sangihe Passage

Abstract The appearance of internal solitary waves (ISWs) in the Maluku Sea is often captured by satellite imagery. However, no study has revealed details on this phenomenon to date. Here, the characteristics of such ISWs were investigated based on their appearance in synthetic aperture radar (SAR) imagery on 20 February 2015. Two different sources of ISW packets were observed: one packet propagating from the Lifamatola Passage and another from the Sangihe Passage. The vertical structure of the waves was constructed using the Korteweg-de Vries (KdV) model, which suggests an average phase speed of ~2.8 and 2.7 m s^{-1} for the first and the second sources, respectively. ISWs originating from the first source had a typical amplitude of O(80 m), while those from the second source were characterized by a lower amplitude of O(40 m). The waves generated horizontal and vertical currents with typical magnitudes of O(1 m s^{-1}) and O(10 cm s^{-1}) for the first source and O(0.6 m s^{-1}) and O(4 cm s^{-1}) for the second source, respectively. The mean energy densities of the first and second sources reached 461 MJ m^{-1} and 185 MJ m^{-1}, respectively. Single leading solitary wave contained a fraction of approximately 20% and 15% of the baroclinic tidal energy generated in the Lifamatola Passage and Sangihe Passage, respectively.

* Corresponding author at: Research Center for Oceanography, National Research and Innovation Agency (RCO-BRIN), Jakarta, Indonesia.
E-mail address: adip003@brin.go.id (A. Purwandana).
Peer review under the responsibility of the Institute of Oceanology of the Polish Academy of Sciences.

Production and hosting by Elsevier

https://doi.org/10.1016/j.oceano.2022.07.008

Please cite this article as: A. Purwandana and Y. Cuypers, Characteristics of internal solitary waves in the Maluku Sea, Indonesia, Oceanologia, https://doi.org/10.1016/j.oceano.2022.07.008

1. Introduction

The Indonesian seas feature hotspots for internal tide generation (Nagai and Hibiya, 2015) as well as internal solitary wave (ISW) formation (Aiki et al., 2011; Chonnaniyah et al., 2021; Purwandana et al., 2021a; Syamsudin et al., 2019). An internal tide is generated when barotropic tidal currents encounter sloping topography, such as a sill (Bouruet-Aubertot et al., 2018; Nagai and Hibiya, 2015). Then, through a nonlinear steepening mechanism (Gerkema, 1996), the slackening of lee waves under supercritical conditions (Alford et al., 2015), or the collision of water masses (Bourgault et al., 2016), ISWs are potentially formed. Their existence can frequently be observed from satellite imagery as bands with a slick pattern (Jackson, 2007; Karang et al., 2012; Mitnik et al., 2000) and can be continuously monitored via an online platform (for example, at https://search.asf.alaska.edu).

ISWs often appear in certain locations within Indonesian waters. Most of the research on ISWs has focused on those observed in the Lombok Strait and Bali waters (Chonnaniyah et al., 2021; Gong et al., 2021; Karang et al., 2012; Purwandana et al., 2021a; Susanto et al., 2005; Syamsudin et al., 2019; Wang et al., 2022). Other locations of interest in ISW studies are the Andaman-Sabang solitary waves (Prasetya et al., 2021; Sun et al., 2021; Vlasenko and Alpers, 2005). However, some identified ISWs in other locations remain uncharacterized, such as those in the Maluku Sea and the Banda Sea.

Several methods can be used to characterize ISW behavior, such as costly field observations and/or time-consuming numerical simulations. To address these limitations, ISW characterization via remote sensing analysis is widely used and benefits from the clear patterns of ISW events identified from satellite imagery (Chonnaniyah et al., 2021; Karang et al., 2020; Lindsey et al., 2018; Mitnik et al., 2000; Vasavi et al., 2021). Although each method may contain certain advantages and disadvantages, different methods can be used to validate each other. A robust method used to infer the subsurface structure of ISWs from satellite images has also been developed and validated by previous studies (Cai et al., 2015; Purwandana et al., 2021b; Wang et al., 2022; Zheng et al., 2001b).

Studying ISW behavior is important for many reasons. These waves serve as a medium that transports internal tidal energy away from their generation sites, which eventually breaks on the shore. This shoaling process is crucial for nearshore ecosystems since the breaking waves enhance the vertical flux of nutrients, thereby increasing the productivity of the pelagic layers (Bourgault et al., 2014, 2007; Helfrich, 1992; Hosegood and Van Haren, 2004; La Forgia et al., 2020, 2019; Masunaga et al., 2015; Moum et al., 2003; Pineda and López, 2002; Venayagamoorthy and Fringer, 2006, 2007; Walter, 2014). ISWs have also been considered a threat to underwater structures and submarines since this phenomenon drives strong horizontal and vertical currents that can disturb the stability and buoyancy of underwater structures (Cui et al., 2019; Dong et al., 2016; Osborne et al., 1978; Zou et al., 2021). Some studies have indicated a possible impact of ISWs on *KRI Nanggala* 402, the Indonesian Navy submarine that was dragged down and sank over a short period of time in northern Bali waters (Gong et al., 2021; Stepanyants, 2021; Wang et al., 2022).

Recently, it was shown that the Maluku Sea is a connector for the western boundary system of the western Pacific Ocean to the internal Indonesian seas via intermediate throughflow and circulation (Yuan et al., 2022). Maluku Sea are also exposed to seasonal winds variability, where southeasterly winds trigger lower sea surface temperature (SST) and phytoplankton bloom hence improving regional fisheries production (Setiawan et al., 2022). However, to date, there is no study on short temporal variability induced by internal tide generation and internal solitary wave events which may affect seawater properties variability in this region. The only observation indicating the existence of internal waves was obtained from an empirical study in the Maluku Sea is a study by Firdaus et al. (2021) using multichannel seismic reflection. Local mixing triggered by strong internal tide generation as well as enhanced mixing due to internal solitary wave breaking are mechanisms which can modify the Pacific water masses properties (Bouruet-Aubertot et al., 2018; Nagai et al., 2021; Nagai and Hibiya, 2015; Purwandana et al., 2020).

This study aimed to tackle the knowledge gap related to ISWs in the Indonesian seas. Among the Indonesian seas, the Maluku Sea is an ISW formation hotspot. However, no study has characterized the existence of ISWs in the Maluku Sea to date. By image analyses of synthetic aperture radar (SAR) image in the Maluku Sea and optimizing a simple Korteweg-de Vries (KdV) model, we reconstructed the substructure of ISWs that could frequently be observed in these waters using a single SAR image containing two different generation sources.

The paper is organized as follows. The methodology is described in Section 2, which contains information on dataset processing including the method used to infer the vertical structure of ISWs as well as aspects of their energetics. Section 3 provides the results and discussion, while Section 4 summarizes the findings of the study.

2. Material and methods

2.1. Subsurface structure of ISWs

In this study, we use the product of Copernicus Sentinel Data that has been previously processed by the European Space Agency (ESA), available to be downloaded at https://search.asf.alaska.edu. The satellite images used in this study were captured by the mission of Sentinel 1-A, beam mode of interferometric wide beam, product type of ground-range detected, high-resolution processing level 1 and polarization type of single VV. The appearance of ISW packet can be viewed almost monthly in the ESA processed images. We spotted the existence of multi-ISW packets which were captured by SAR imagery on 11 October 2014 at 21:17 local time (hereafter SAR-1410) and on 20 February 2015 at 21:17 local time (hereafter SAR-1502) in the Maluku Sea. Both images covered the Maluku Sea and contained distinguishable ISW packets (Figure 1a). A deep analysis involving simple remote sensing data analyses was used to investigate the characteristics of these waves. In this study, we focused on the image SAR-1502.

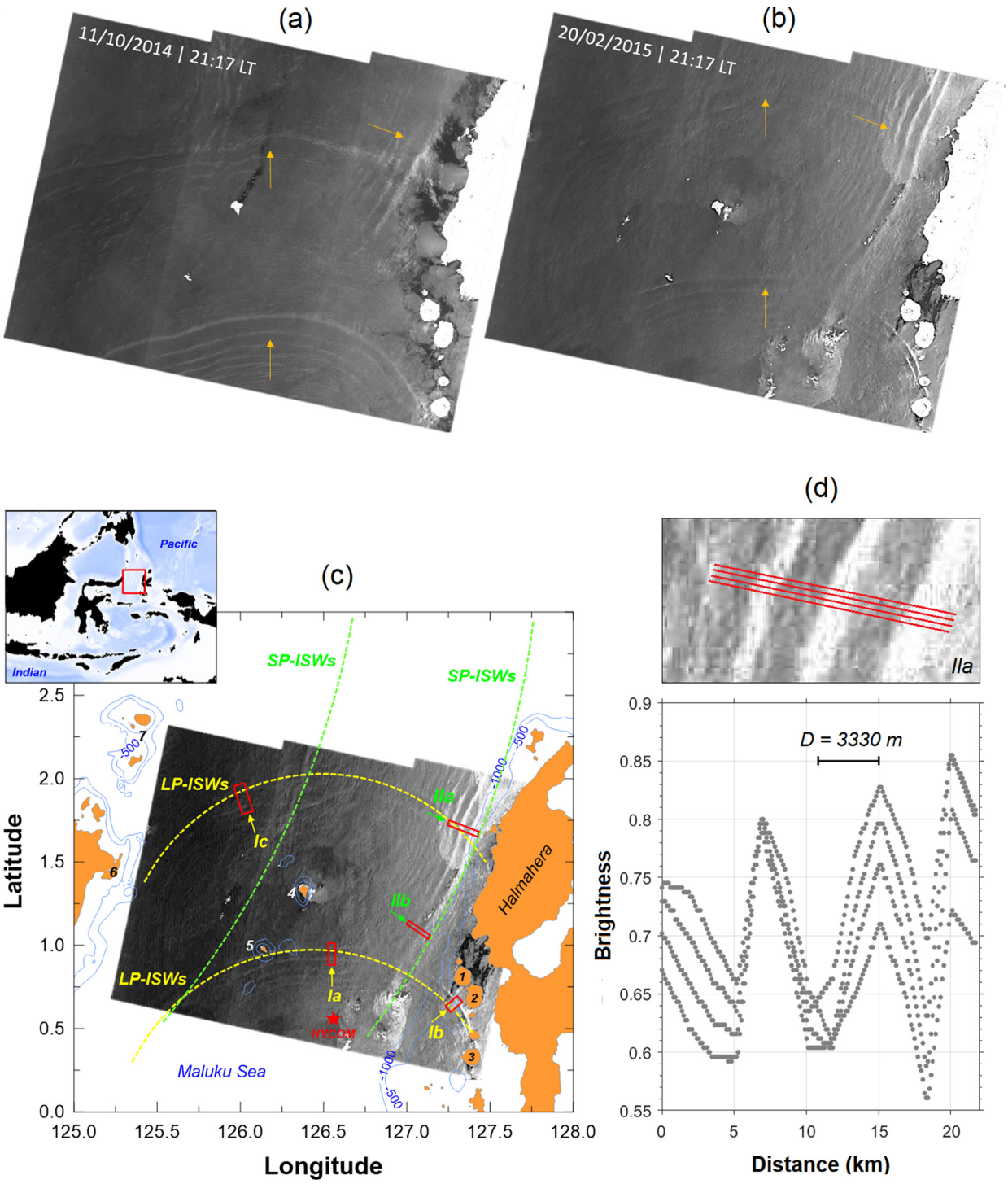

Figure 1 (a) Exclusive appearance of two different sources (northward and eastward, yellow arrows) of ISW packets within synthetic aperture radar (SAR) images (https://search.asf.alaska.edu) taken of the Maluku Sea on 11 October 2014 at 21:17 local time and (b) on 20 February 2015 at 21:17 local time. (c) SAR image analyzed in this study (20 February 2015) overlaid on GEBCO topography. The red star denotes the hybrid coordinate ocean model (HYCOM) station (126.5601°E; 0.5600°N) used to reconstruct the underwater structure of the wave (https://hycom.org/dataserver/gofs-3pt1/analysis). Roman numerals *I* and *II* represent the wave packets propagating from the Lifamatola Passage and Sangihe Passage, respectively. The letters *a*, *b*, and *c* denote the locations of the ISW investigation. The red boxes represent the areas used to infer the half-width of the waves via brightness scaling analysis. The yellow and green dashed curves denote the wave arc lines of the LP-ISW ($\Lambda = 272.41$ km) and SP-ISW ($\Lambda = 313.55$ km) used to calculate per tidal energy flux. (d) The identification process of the ISW signature *D*, the distance between the center of the bright and dark bands within the SAR image taken on 20 February 2015 at 21:17 local time (upper panel), and the brightness level (arbitrary unit) variability along the red lines (lower panel). The Islands surrounding the Maluku Sea are also indicated: (1) Ternate, (2) Tidore, (3) Makian, (4) Maju, (5) Gureda, (6) Lembeh and (7) Sangihe.

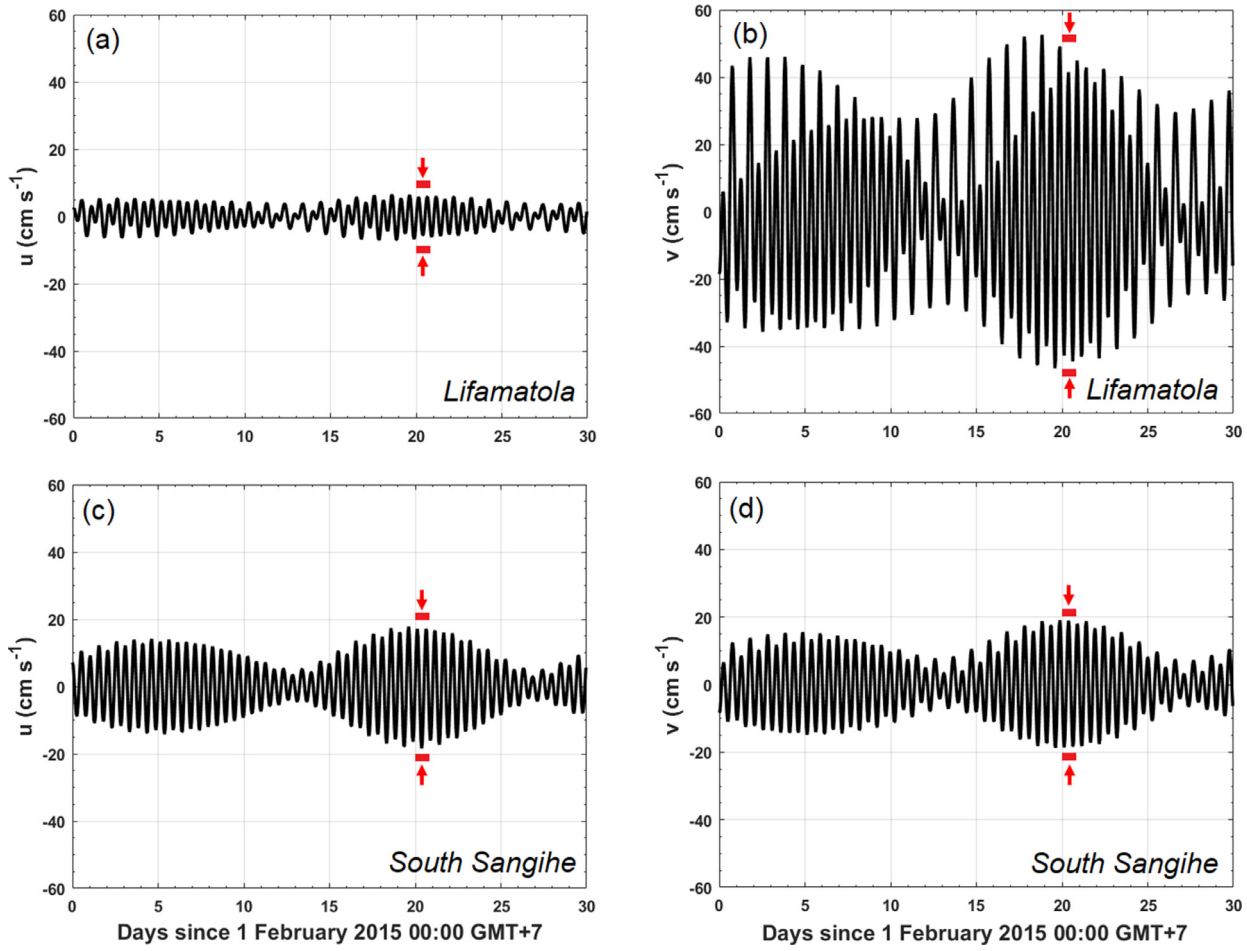

Figure 2 Predicted tides inferred from Oregon State University tidal inversion software (OTIS) (Egbert and Erofeeva, 2002) for February 2015 at Lifamatola Passage (126.8514°E; 1.8296°S) and Sangihe Passage (125.3361°E; 1.8509°N), for the zonal current component (u, cm s^{-1}) in the (a) Lifamatola Passage and (b) South Sangihe Passage, and for the meridional current component (v, cm s^{-1}) in the (c) Lifamatola Passage and (d) Sangihe Passage. Red arrows indicate the timing of the observed internal solitary wave (ISW) packets shown in Figure 1 (20 February 2015).

Sea surface roughness presented by the convergence and divergence of ISWs is often manifested as bright and dark bands in the wave front and rear, respectively (Mitnik et al., 2000). As shown in Figure 1b—c, the signatures of ISWs were observed during the spring tide period in the Lifamatola Passage (hereafter LP, considered the first source of the northward propagating ISWs, Figure 2a—b) and in the Sangihe Passage (hereafter SP, considered the second source of the eastward propagating ISWs, Figure 2c—d).

The subsurface structures of the ISWs were reconstructed by employing a single station for temperature and salinity profiles obtained from the Hybrid Coordinate Ocean Model (HYCOM), which has 0.08° grid resolution products at 126.5601°E; 0.5600°N for 20 February 2015 (https://hycom.org/dataserver/gofs-3pt1/analysis) (Figure 3b). Theoretically, a solitary wave creates its shape following the classical $sech^2$ solitary wave solution of the Korteweg-de Vries (KdV) equation, where the nonlinear and dispersive terms balance each other to maintain the shape of the wave. The KdV equation in a stratified fluid (Ostrovsky and Stepanyants, 1989) is expressed as:

$$\frac{\partial \eta}{\partial t} + c\frac{\partial \eta}{\partial x} + \alpha\eta\frac{\partial \eta}{\partial x} + \beta\frac{\partial^3 \eta}{\partial^3 x} = 0 \quad (1)$$

where $\eta(x,t)$ is the maximum vertical displacement of the isopycnal for a vertical mode-1 wave calculated from the stratification profile (Holloway et al., 1997), x is distance, and t is time. A classical solution to this equation is:

$$\eta = \eta_0 sech^2\left[\frac{(c_1 + \frac{\alpha\eta_0}{3})(t_0 - t)}{\Delta}\right] \quad (2)$$

The term $(c_1+\alpha\eta_0/3)$ is known as the phase speed (C_p) term of the wave. c_1 is the mode-1 linear phase speed as a function of the density gradient and layer thickness between the upper and lower layer separated by the center of the pycnocline layer (Zhang et al., 2022; Zheng et al., 2001a), also known as the Eigen speed of the Sturm-Liouville equation of the mode-1 vertical Eigen function or vertical structure of the displacement amplitude of the wave, $\Phi(z)$:

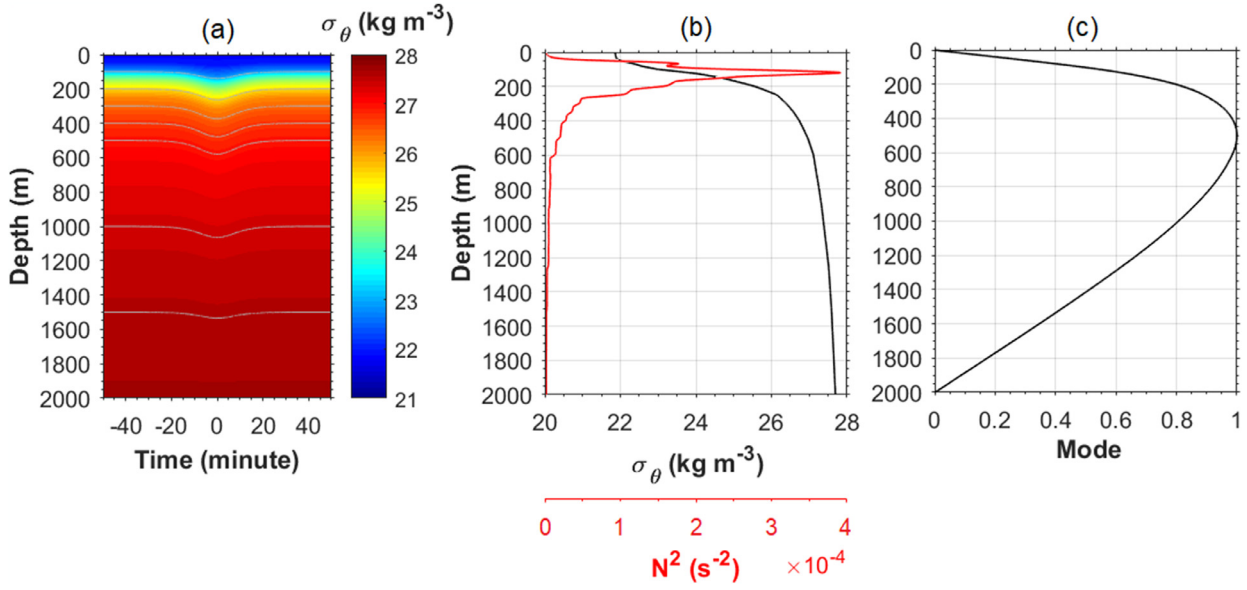

Figure 3 (a) Density perturbation during the passage of an ISW, reconstructed using the KdV solution for LP-ISW *Ia* ($\eta_0 = 79.78$ m). (b) Potential density (black) and squared buoyancy frequency (red) profiles from HYCOM products (126.5601°E; 0.5600°N) on 20 February 2015 (https://hycom.org/dataserver/gofs-3pt1/analysis). (c) Mode-1 vertical structure of the ISW inferred from the density profile.

$$\frac{d^2\Phi}{dz^2} + \frac{N^2(z)}{c_1^2}\Phi = 0 \tag{3}$$

Here, we applied the boundary conditions $\Phi(0) = \Phi(-H) = 0$. N^2 represents the background stratification inferred from the density profile (Figure 3b), η_0 is the ISW amplitude derived from the ISW band with a bright-dark pattern in the SAR image (Holloway et al., 1997; Zheng et al., 2001b):

$$\eta_0 = \frac{12\beta}{\alpha\Delta^2} = 1.32^2\frac{12\beta}{\alpha D^2} \tag{4}$$

Here, D is the distance between the center of the bright and dark bands (see Figure 1d), while Δ is the half-width of the wavelength, expressed as $\Delta^2 = 12\beta/(\alpha\eta_0)$. Notably, the constant of proportionality (1.32^2) in Eq. (3) was obtained from an empirical study (Zheng et al., 2001b). α and β are the nonlinear and dispersion coefficients, respectively, as calculated by Holloway et al. (1997):

$$\alpha = \left(\frac{3}{2}\right)\frac{\int_{-H}^{0}(c_1-U)^2(d\Phi/dz)^3dz}{\int_{-H}^{0}(c_1-U)\,(d\Phi/dz)^2dz}dz \tag{5}$$

$$\beta = \left(\frac{1}{2}\right)\frac{\int_{-H}^{0}(c_1-U)^2\Phi^2dz}{\int_{-H}^{0}(c_1-U)\,(d\Phi/dz)^2dz}dz \tag{6}$$

where U is the background current. In absence of an in-situ dataset, the term U was neglected in this study.

An ISW drives velocity fields in both horizontal and vertical extents. By employing the mode-1 Eigen function, these 'pseudo' currents were estimated using the method of Cai et al. (2015):

$$u = C_p\frac{d\Phi}{dz}sech^2\left[\frac{(c_1+\frac{\alpha\eta_0}{3})(t_0-t)}{\Delta}\right] \tag{7}$$

$$w = \frac{d\eta}{dt} \tag{8}$$

where u and w are velocities in the horizontal and vertical directions, respectively. Notably, the horizontal direction of u is the same as the direction of the propagation.

2.2. Energetics of the ISW

The energetic properties of the wave were estimated using the density perturbation created by the ISW and the current fields computed by Eq. (7) and Eq. (8). The energy of an ISW is composed of the available potential energy (APE) and the kinetic energy (KE). The density of the APE per unit length was computed by integrating over the vertical and horizontal extent of an ISW as follows:

$$\text{APE} = \int_{-L}^{L}\int_{-H}^{0}\int_{0}^{\eta(z)}\rho(z)N^2(z')z'dz'dzdx \tag{9}$$

The density of the KE per unit length of the ISW was computed as:

$$\text{KE} = \frac{1}{2}\int_{H}^{0}\int_{-L}^{L}\rho\left(u^2+w^2\right)dxdz \tag{10}$$

3. Results and discussion

3.1. Subsurface structures of the ISWs

As shown in Figure 1a–b, the ISW crests covered nearly the entire region of the Maluku Sea. The ISW events captured by the SAR-1502 image presented here were observed on 20 February 2015 during the spring tide period (see Figure 2). The LP-ISW packets propagated northward, with their crests spanning from Sulawesi Island on the western side to Halmahera Island on the eastern side, covering more than 270 km in length. The SP-ISW packets covered the northern part of the Maluku Sea, propagating eastward

and eventually breaking on the western coast of Halmahera Island. The ISW packets performed as rank-ordered solitary waves and contained up to 4–5 solitary waves (see Figure 1a–b) with a decreasing brightness trend, from the front to the rear of the packet. In both SAR-1410 and SAR-1502 images, we observed two packets of ISWs emanating from the LP and SP. The distance between the two leading waves (dashed curves in Figure 1c) for the LP-ISWs and SP-ISWs was ~120 km. With such a distance and a semidiurnal tidal period of 12.41 hours, this gives a phase speed of ~2.7 m s^{-1}.

Using Eqs. (2)–(6), we estimated the typical amplitude of the ISWs in the Maluku Sea to be in the order of 80 m for the LP-ISW and 40 m for the SP-ISW. The typical half-width of the waves was ~1800 m for the LP-ISW and ~2500 m for the SP-ISW (see Table 1 for details). From the KdV framework, we can also estimate that the typical phase speed of the LP-ISWs and SP-ISWs was ~2.8 and ~2.7 m s^{-1}, respectively which is in good agreement with the independent estimate obtained from satellite imagery.

Internal tide modeling studies by Nagai and Hibiya (2015) and Nugroho et al. (2016) have also shown the existence of two propagation sources of M_2 internal tide in the Maluku Sea, i.e. the northward propagation from the Lifamatola Passage and the eastward propagation from the Sangihe Passage. The existence of these two sources is characterized by a strong conversion rate from barotropic to baroclinic tides and strong M_2 baroclinic energy fluxes. This conversion from barotropic to baroclinic tides results from the interaction of the relatively strong M_2 barotropic flow with the rough topography of LP and SP which forces isopycnal oscillation at the M_2 frequency.

As can be inferred from Figure 2, the barotropic velocities $U_{bar} = \sqrt{u^2 + v^2}$ in the LP and SP reached ~0.5 and ~0.3 m s^{-1}, respectively. The mode-1 phase speed inferred from the stratification profile in the Maluku Sea c_1 was 2.49 m s^{-1}, resulting in Froude numbers $Fr = U_{bar}/c_1$ of 0.20 and 0.12 ($Fr < 1$) for the LP and SP, respectively. These results exclude the possibility of ISW formation through a lee wave mechanism (Maxworthy, 1979). We hypothesize that the generation of ISWs in these waters occurs through the nonlinear steepening effect of the waves of depression in the pycnocline layer. Notably, the ISW packets that propagated from the LP (*Ia*) and SP (*IIa*) were located ~310 and ~225 km away from the generation sites in the LP and SP, respectively, which also supports our hypothesis.

Internal tides are formed when a barotropic tidal current encounters shallowing topography such as sills and forces isopycnal oscillation resulting in conversion from barotropic to baroclinic (internal) tides (Baines, 1982). For large internal tides, non-linear and non-hydrostatic processes can then break internal tides into a sequence of ISWs following the steepening mechanism or the lee wave mechanism (Alford et al., 2015).

A common feature accompanying the solitary wave events was an isopleth or bulb of strong current in both horizontal and vertical directions. The maximum horizontal and vertical currents triggered by the waves are shown in Table 1. The LP-ISWs were characterized by a magnitude of horizontal and vertical currents two times and three times higher, respectively, compared to those of the SP-ISWs. As shown in Figure 4 (u, uppermost panel), the strong hori-

Table 1 The characteristics of the internal solitary waves (ISWs) in the Maluku Sea. The species of the ISWs being investigated refer to Figure 1.

ISW	D (m)	Δ (m)	c_1 (m s^{-1})	α (s^{-1})	β (m^3 s^{-1})	η_0 (m)	C_p (m s^{-1})	U_{max} (m s^{-1})	w_{max} (cm s^{-1})	Energy (MJ m^{-1})		
										KE	APE	KE/APE
Ia	2391	1813	2.49	-1.28×10^{-2}	2.81×10^5	79.78	2.83	1.14	9.6	291.7	181.7	1.61
Ib	2476	1877				74.40	2.81	1.06	8.6	257.5	166.5	1.55
Ic	2370	1797				81.20	2.84	1.17	9.9	301.1	185.8	1.62
IIa	3330	2525				41.13	2.67	0.56	3.3	93.3	78.2	1.19
IIb	3170	2404				45.39	2.69	0.62	3.9	110.0	88.8	1.24

Table 2 Fraction of ISW energy estimates based on previous barotropic to internal tide energy conversion and dissipation study by Nagai and Hibiya (2015).

Region	Energy Conversion (GW)	Local Dissipation Energy (GW/%)	Single ISW Energy* (GW/%)
Seram Sea-Lifamatola Passage	14.3	9.4/65.7%	2.81/19.7%
Sangihe Passage	7.8	3.8/48.7%	1.20/15.4%

* This study

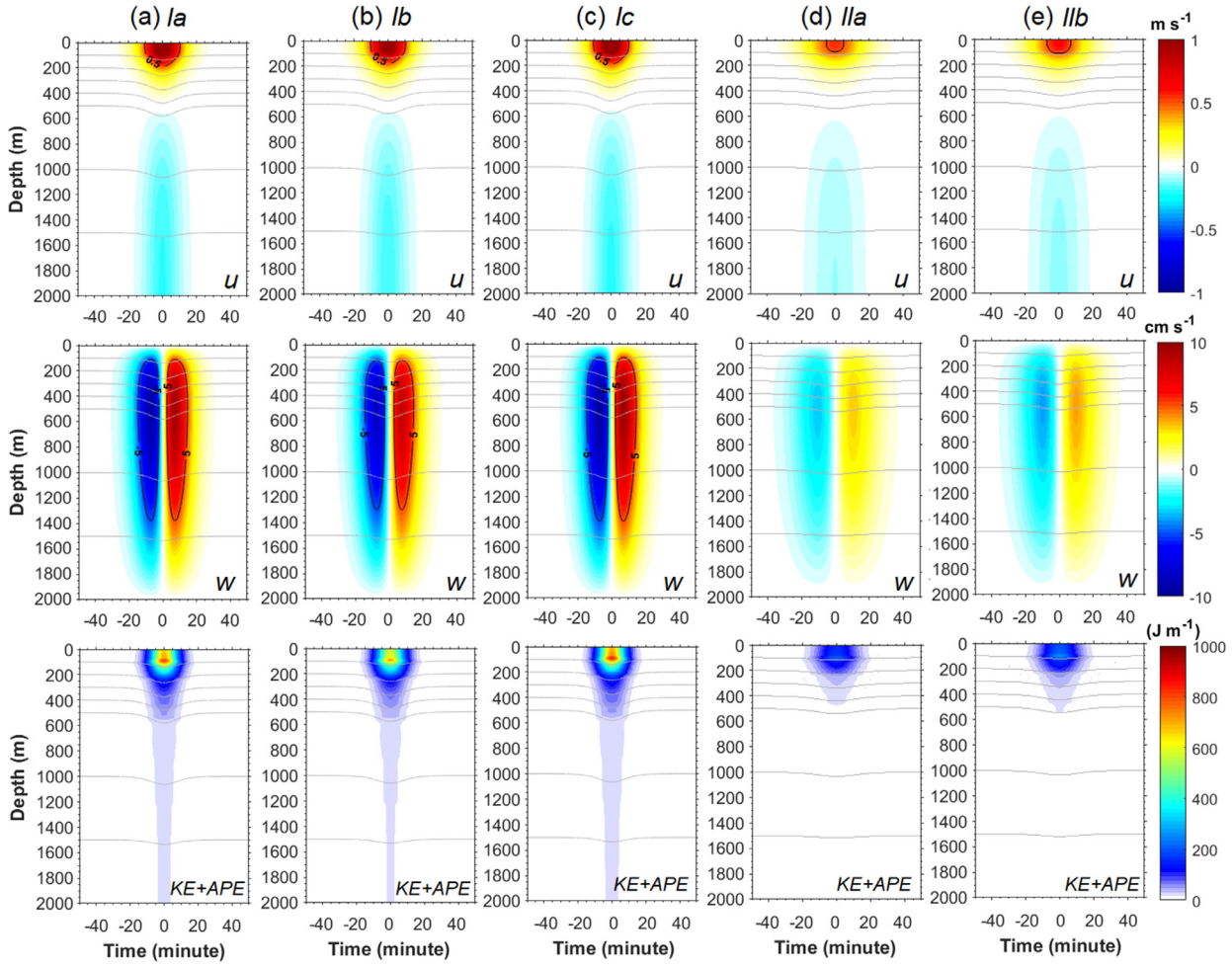

Figure 4 (a) Horizontal velocity (u, uppermost panel), (b) vertical velocity (w, middle panel), and (c) total energy density (KE+APE, lower panel). Gray lines represent the KdV fits at several depths (100, 200, 300, 400, 500, 1000, and 1500 m). Black contour lines of a horizontal/vertical velocity of 0.5 m s^{-1}/5 cm s^{-1} are shown. The properties of the KdV fits are shown in Table 1.

zontal currents extended up to ~400 m in depth, while the core of velocity greater than 0.5 m s^{-1} occurred in the upper 200 m for the LP-ISWs and the upper 100 m for the SP-ISWs. The typical maximum horizontal velocities of the LP-ISWs and SP-ISWs were 1.1 m s^{-1} and 0.6 m s^{-1}, respectively. The maximum velocities of the LP-ISWs were higher than that observed in Bali waters (0.65 m s^{-1}; Wang et al., 2022) but for the SP-ISWs, the maximum velocities were comparable to that observed in the Bali waters. Below 600 m depth, the opposite direction of velocity was observed. A typical downward-upward direction of vertical velocity occurred before and after the trough of the waves, with typical maximum velocities of ~10 cm s^{-1} and 4 cm s^{-1} for the LP-ISWs and SP-ISWs, respectively. This extended down to ~2000 m, with the core of velocity greater than 5 cm s^{-1} covering a depth from 100 to 1400 m. These values are comparable to those observed for ISWs within the Lombok Strait (Purwandana et al., 2021a; Wang et al., 2022).

3.2. Energetics

The energy contained in each ISW was computed using the fitted solution of the KdV solution. The KE and APE for each wave representing some areas of interest within the

ISW packets are shown in Table 1. The mean KE/APE ratios were typically 1.6 and 1.2 for the LP-ISWs and SP-ISWs, respectively, which are close to the values reported in the literature (Klymak et al., 2006). The total energy density (KE+APE) reached 461 and 185 MJ m^{-1} for the LP-ISWs and SP-ISWs, respectively. This value is approximately one-third of that observed for an ISW in the South China Sea (Klymak et al., 2006), yet two orders of magnitude larger than the values observed for ISWs on the Oregon Shelf (Moum et al., 2007). The vertical structure of the KE + APE for each wave is shown in Figure 4 (lowest panel).

A clear shape of the arc front of the ISW packets enabled us to determine the energy brought by the waves. Considering the conservation of total energy flux $F_{tot} = C_p \frac{KE+APE}{2\Delta} \Lambda$ and the arc front (Λ) of the waves being 272.41 and 313.55 km for the LP-ISW and SP-ISW, respectively (see Figure 1, yellow and green dashed curves), a mean energy flux per tidal cycle (12.41 hours) of ~2.81 GW and ~1.20 GW was carried by the first leading ISW of the packet for the LP-ISWs and SP-ISWs, respectively. We could not precisely estimate the amplitude of all waves in each packet due to the limited image resolution of the SAR images. The energy flux values observed in this study are higher than those reported for ISW packets observed in the Lombok Strait (1.59 GW) formed by the regular semidiurnal M_2 internal tides generated above the Nusa Penida Sill (Aiki et al., 2011). Considering that the barotropic to baroclinic tidal energy conversion in the LP and SP is 14.3 GW and 7.8 GW, respectively (Nagai and Hibiya, 2015), the energy flux carried by ISW represents a large fraction of the internal tide energy conversion. Table 2 presents the fraction of energy conversion from baroclinic tidal energy into a single solitary wave front in the LP and SP, respectively. Notably, there is a possibility for energy dissipation during the propagation due to the variable topography and small islands in the center of the Maluku Sea (i.e., the Islands of Maju and Gureda, Figure 1c).

4. Conclusions

Through a coupling analysis involving satellite imagery and KdV solution, we found significant amplitudes of ISWs in the Maluku Sea. There were at least two ISW packets from different sources of generation from the Lifamatola Passage and Sangihe Passage, which traveled northward and eastward, respectively. The waves propagated with a typical phase speed of 2.7–2.8 m s^{-1} and triggered strong horizontal and vertical velocities of up to 1 m s^{-1} and 10 cm s^{-1}, respectively. Our phase speed estimates using the KdV solution were validated by the satellite images, which confirmed that the ISW packets were generated every 12.41 hours.

The ISWs observed in this study are not among the highest amplitude underwater waves confirmed in the Indonesian seas. Compared to ISWs observed in other locations, the amplitudes of the Maluku ISWs (LP-ISW: O(80 m); SP-ISW: O(40 m)) are comparable to those frequently observed near the Lombok coast in the Lombok Strait through direct observations (O(40 m); Purwandana et al., 2021a), a theoretical approach employing SAR images and the KdV model (O(41 m); Wang et al., 2022), and an approach using numerical modeling (O(60–90 m); Aiki et al., 2011; Gong et al., 2021). The highest ISW amplitude revealed from direct observations was approximately 185 m in the Lombok Strait, which was considered as an extreme event that is known to be the highest amplitude ever recorded in the Indonesian seas (Pushidrosal, 2021).

This study provides the first characterization of ISWs in the Maluku Sea and highlights the extraordinary activity of a solitary wave event in these waters that could pose risks to submarine navigation and other underwater activities. Notably, further investigations involving in situ observations are required to cross-validate the KdV estimates as well as their fate when shoaling off western Halmahera Island. A significant ISW breaking along the coastal region of western Halmahera Island may induce strong mixing, which is an important mechanism that controls vertical nutrient flux and sediment resuspension.

Declaration of Competing Interest

None.

Acknowledgement

This project is funded by the research scheme of *Program Riset Unggulan* COREMAP CTI 2021–2022 (17/A/DK/2021). We also thank Institute of Oceanology of Polish Academy of Sciences for funding the publication of this research.

References

Aiki, H., Matthews, J.P., Lamb, K.G., 2011. Modeling and energetics of tidally generated wave trains in the Lombok Strait: Impact of the Indonesian Throughflow. J. Geophys. Res.-Oceans 116. https://doi.org/10.1029/2010JC006589

Alford, M.H., Peacock, T., Mackinnon, J.A., Nash, J.D., Buijsman, M.C., Centuroni, L.R., Chao, S.Y., Chang, M.H., Farmer, D.M., Fringer, O.B., Fu, K.H., Gallacher, P.C., Graber, H.C., Helfrich, K.R., Jachec, S.M., Jackson, C.R., Klymak, J.M., Ko, D.S., Jan, S., Johnston, T.M.S., Legg, S., Lee, I.H., Lien, R.C., Mercier, M.J., Moum, J.N., Musgrave, R., Park, J.H., Pickering, A.I., Pinkel, R., Rainville, L., Ramp, S.R., Rudnick, D.L., Sarkar, S., Scotti, A., Simmons, H.L., St Laurent, L.C., Venayagamoorthy, S.K., Wang, Y.H., Wang, J., Yang, Y.J., Paluszkiewicz, T., Tang, T.Y., 2015. The formation and fate of internal waves in the South China Sea. Nature 521, 65–69. https://doi.org/10.1038/nature14399

Baines, P.G., 1982. On internal tide generation models. Deep Sea Res. Pt. A 29, 307–338. https://doi.org/10.1016/0198-0149(82)90098-X

Bourgault, D., Blokhina, M.D., Mirshak, R., Kelley, D.E., 2007. Evolution of a shoaling internal solitary wavetrain. Geophys. Res. Lett. 34, 1–5. https://doi.org/10.1029/2006GL028462

Bourgault, D., Galbraith, P.S., Chavanne, C., 2016. Generation of internal solitary waves by frontally forced intrusions in geophysical flows. Nat. Commun. 7. https://doi.org/10.1038/ncomms13606

Bourgault, D., Morsilli, M., Richards, C., Neumeier, U., Kelley, D.E., 2014. Sediment resuspension and nepheloid layers induced by long internal solitary waves shoaling orthogonally on uniform slopes. Cont. Shelf Res. 72, 21–33. https://doi.org/10.1016/j.csr.2013.10.019

Bouruet-Aubertot, P., Cuypers, Y., Ferron, B., Dausse, D., Ménage, O., Atmadipoera, A., Jaya, I., 2018. Contrasted turbulence intensities in the Indonesian Throughflow: a challenge for parameterizing energy dissipation rate. Ocean Dyn. 68, 779—800. https://doi.org/10.1007/s10236-018-1159-3

Cai, S., Xu, J., Liu, J., Chen, Z., Xie, J., Li, J., He, Y., 2015. Retrieval of the maximum horizontal current speed induced by ocean internal solitary waves from low resolution time series mooring data based on the KdV theory. Ocean Eng. 94, 88—93. https://doi.org/10.1016/j.oceaneng.2014.11.023

Chonnaniyah, Karang, I.W.G.A., Osawa, T., 2021. Internal solitary waves propagation speed estimation in the northern-part of Lombok Strait observed by Sentinel-1 SAR and Himawari-8 images. IOP Conf. Ser. Earth Environ. Sci. 944. https://doi.org/10.1088/1755-1315/944/1/012042

Cui, J., Dong, S., Wang, Z., Han, X., Yu, M., 2019. Experimental research on internal solitary waves interacting with moored floating structures. Mar. Struct. 67, 102641. https://doi.org/10.1016/j.marstruc.2019.102641

Dong, M.S., Tian, X.F., Yuan, Z., Fei, T., 2016. Vibration Control of the Submerged Floating Tunnel under Combined effect of Internal Wave and Ocean Current. Procedia Eng. 166, 160—170. https://doi.org/10.1016/j.proeng.2016.11.579

Egbert, G.D., Erofeeva, S.Y., 2002. Efficient Inverse Modeling of Barotropic Ocean Tides. J. Atmos. Ocean. Technol. 19, 183—204. https://doi.org/10.1175/1520-0426(2002)019<0183:EIMOBO>2.0.CO;2

Firdaus, R., Manik, H.M., Atmadipoera, A.S., Zuraida, R., Purwanto, R., 2021. Imaging thermohaline fine structure using multichannel seismic reflection in the northern Maluku Sea. J. Ilmu dan Teknol. Kelaut. Trop. 13, 151—162. https://doi.org/10.29244/jitkt.v13i1.32346

Gerkema, T., 1996. A unified model for the generation and fission of internal tides in a rotating ocean. J. Mar. Res. 54, 421—450. https://doi.org/10.1357/0022240963213574

Gong, Y., Xie, J., Xu, J., Chen, Z., He, Y., Cai, S., 2021. Oceanic internal solitary waves at the Indonesian submarine wreckage site. Acta Oceanol. Sin. 41, 1—5. https://doi.org/10.1007/s13131-021-1893-0

Helfrich, K.R., 1992. Internal solitary shoaling and breaking on a uniform slope. J. Fluid Mech. 243, 133—154. https://doi.org/10.1017/S0022112092002660

Holloway, P., Pelinovsky, E., Talipova, T., Barnes, B., 1997. A nonlinear model of internal tide transformation on the Australian North West Shelf. J. Phys. Oceanogr. 27, 871—896. https://doi.org/10.1175/1520-0485(1997)027<0871:ANMOIT>2.0.CO;2

Hosegood, P., Van Haren, H., 2004. Near-bed solibores over the continental slope in the Faeroe-Shetland Channel. Deep. Res. Pt. II Top. Stud. Oceanogr. 51, 2943—2971. https://doi.org/10.1016/j.dsr2.2004.09.016

Jackson, C., 2007. Internal wave detection using the Moderate Resolution Imaging Spectroradiometer (MODIS). J. Geophys. Res. 112, C11012. https://doi.org/10.1029/2007JC004220

Karang, I.W.G.A., Chonnaniyah, Osawa, T., 2020. Internal solitary wave observations in the Flores Sea using the Himawari-8 geostationary satellite. Int. J. Remote Sens. 41, 5726—5742. https://doi.org/10.1080/01431161.2019.1693079

Karang, I.W.G.A., Nishio, F., Mitnik, L., Osawa, T., 2012. Spatial-Temporal Distribution and Characteristics of Internal Waves in the Lombok Strait Area Studied by Alos-Palsar Images. Earth Sci. Res. 1, 11—22. https://doi.org/10.5539/esr.v1n2p11

Klymak, J.M., Pinkel, R., Liu, C.T., Liu, A.K., David, L., 2006. Prototypical solitons in the South China Sea. Geophys. Res. Lett. 33, 5—8. https://doi.org/10.1029/2006GL025932

La Forgia, G., Adduce, C., Falcini, F., Paola, C., 2019. Migrating Bedforms Generated by Solitary Waves. Geophys. Res. Lett. 46, 4738—4746. https://doi.org/10.1029/2019GL082511

La Forgia, G., Tokyay, T., Adduce, C., Constantinescu, G., 2020. Bed shear stress and sediment entrainment potential for breaking of internal solitary waves. Adv. Water Resour. 135, 103475. https://doi.org/10.1016/j.advwatres.2019.103475

Lindsey, D.T., Nam, S.H., Miller, S.D., 2018. Tracking oceanic nonlinear internal waves in the Indonesian seas from geostationary orbit. Remote Sens. Environ. 208, 202—209. https://doi.org/10.1016/j.rse.2018.02.018

Masunaga, E., Homma, H., Yamazaki, H., Fringer, O.B., Nagai, T., Kitade, Y., Okayasu, A., 2015. Mixing and sediment resuspension associated with internal bores in a shallow bay. Cont. Shelf Res. 110, 85—99. https://doi.org/10.1016/j.csr.2015.09.022

Maxworthy, T., 1979. Note on the Internal Solitary Waves Produced By Tidal Flow Over a Three-Dimensional Ridge. J. Geophys. Res. 84, 338—346. https://doi.org/10.1029/jc084ic01p00338

Mitnik, L., Alpers, W., Hock, L., 2000. Thermal plumes and internal solitary waves generated in the Lombok strait studied by ERS SAR. Eur. Sp. Agency, (Special Publ. ESA SP) 1834—1842.

Moum, J.N., Farmer, D.M., Smyth, W.D., Armi, L., Vagle, S., 2003. Structure and Generation of Turbulence at Interfaces Strained by Internal Solitary Waves Propagating Shoreward over the Continental Shelf. J. Phys. Oceanogr. 33, 2093—2112. https://doi.org/10.1175/1520-0485(2003)033<2093:SAGOTA>2.0.CO;2

Moum, J.N., Klymak, J.M., Nash, J.D., Perlin, A., Smyth, W.D., 2007. Energy transport by nonlinear internal waves. J. Phys. Oceanogr. 37, 1968—1988. https://doi.org/10.1175/JPO3094.1

Nagai, T., Hibiya, T., 2015. Internal tides and associated vertical mixing in the Indonesian Archipelago. J. Geophys. Res.-Oceans 120, 3373—3390. https://doi.org/10.1002/2014JC010592

Nagai, T., Hibiya, T., Syamsudin, F., 2021. Direct Estimates of Turbulent Mixing in the Indonesian Archipelago and Its Role in the Transformation of the Indonesian Throughflow Waters. Geophys. Res. Lett. 48, e2020GL091731. https://doi.org/10.1029/2020GL091731

Nugroho, D., Koch-Larrouy, A., Gaspar, P., Lyard, F., Reffray, G., Tranchant, B., 2016. Modelling explicit tides in the Indonesian seas: An important process for surface sea water properties. Mar. Pollut. Bull. https://doi.org/10.1016/j.marpolbul.2017.06.033

Osborne, A.R., Burch, T.L., Scarlet, R.I., 1978. The Influence Of Internal Waves On Deepwater Drilling Operations. J. Pet. Technol. 30, 1497—1504. https://doi.org/10.4043/2797-MS

Ostrovsky, L.A., Stepanyants, Y.A., 1989. Do internal solitions exist in the ocean? Rev. Geophys. 27, 293—310. https://doi.org/10.1029/RG027i003p00293

Pineda, J., López, M., 2002. Temperature, stratification and barnacle larval settlement in two Californian sites. Cont. Shelf Res. 22, 1183—1198. https://doi.org/10.1016/S0278-4343(01)00098-X

Prasetya, I.A., Atmadipoera, A.S., Budhiman, S., Nugroho, U.C., 2021. Internal solitary waves in the Northwest Sumatra Sea-Indonesia: From observation and modeling. IOP Conf. Ser. Earth Environ. Sci. 944. https://doi.org/10.1088/1755-1315/944/1/012056

Purwandana, A., Cuypers, Y., Bouruet-Aubertot, P., 2021a. Observation of internal tides, nonlinear internal waves and mixing in the Lombok Strait. Indonesia. Cont. Shelf Res. 216. https://doi.org/10.1016/j.csr.2021.104358

Purwandana, A., Cuypers, Y., Bouruet-Aubertot, P., Nagai, T., Hibiya, T., Atmadipoera, A.S., 2020. Spatial structure of turbulent mixing inferred from historical CTD datasets in the Indonesian seas. Prog. Oceanogr. 184, 102312. https://doi.org/10.1016/j.pocean.2020.102312

Purwandana, A., Cuypers, Y., Kusmanto, E., Bouruet-Aubertot, P., Rachman, A., Muhadjirin, Dwi, Santoso, P., 2021b. Observed internal solitary waves in the western Halmahera Sea, Indonesia. In: The 2nd International Symposium on Physics and Appli-

cations (ISPA). Department of Physics, Faculty of Sciences and Data Analytics. Institut Teknologi Sepuluh Nopember, Indonesia, Surabaya, 38.

Pushidrosal, 2021. World Hydrography Day 2021— International Webinar (Pushidrosal Channel — YouTube).

Setiawan, R.Y., Iskandar, I., Wirasatriya, A., R, D.S., Siswanto, E., Pranowo, W.S., Setiawati, M.D., Mardiansyah, W., 2022. Seasonal and interannual coastal wind variability off the central Maluku Islands revealed by satellite oceanography. Glob. NEST J. 24, 37—43. https://doi.org/10.30955/gnj.004177

Stepanyants, Y., 2021. How internal waves could lead to wreck American and Indonesian submarines? Cornell Univ., 28 pp. https://doi.org/10.48550/arXiv.2107.00828

Sun, L., Zhang, J., Meng, J., 2021. Study on the propagation velocity of internal solitary waves in the Andaman Sea using Terra/Aqua-MODIS remote sensing images. J. Oceanol. Limnol. 39, 2195—2208. https://doi.org/10.1007/s00343-020-0280-6

Susanto, R.D., Mitnik, L., Zheng, Q., 2005. Ocean Internal Waves Observed in the Lombok Strait. Oceanography 18, 80—87. https://doi.org/10.5670/oceanog.2005.08

Syamsudin, F., Taniguchi, N., Zhang, C., Hanifa, A.D., Li, G., Chen, M., Mutsuda, H., Zhu, Z.N., Zhu, X.H., Nagai, T., Kaneko, A., 2019. Observing Internal Solitary Waves in the Lombok Strait by Coastal Acoustic Tomography. Geophys. Res. Lett. 46, 10475—10483. https://doi.org/10.1029/2019GL084595

Vasavi, S., Divya, C., Sarma, A.S., 2021. Detection of solitary ocean internal waves from SAR images by using U-Net and KDV solver technique. Glob. Transitions Proc. 2, 145—151. https://doi.org/10.1016/j.gltp.2021.08.063

Venayagamoorthy, S.K., Fringer, O.B., 2007. On the formation and propagation of nonlinear internal boluses across a shelf break. J. Fluid Mech. 577, 137—159. https://doi.org/10.1017/S0022112007004624

Venayagamoorthy, S.K., Fringer, O.B., 2006. Numerical simulations of the interaction of internal waves with a shelf break. Phys. Fluids 18. https://doi.org/10.1063/1.2221863

Vlasenko, V., Alpers, W., 2005. Generation of secondary internal waves by the interaction of an internal solitary wave with an underwater bank. J. Geophys. Res.-Oceans 110, 1—16. https://doi.org/10.1029/2004JC002467

Walter, R.K., 2014. Nonlinear internal waves, internal bores, and turbulent mixing in the nearshore coastal environment. Diss. Univ. Stanford, 264 pp.

Wang, T., Huang, X., Zhao, W., Zheng, S., Yang, Y., Tian, J., 2022. Internal Solitary Wave Activities near the Indonesian Submarine Wreck Site Inferred from Satellite Images. J. Mar. Sci. Eng. 10. https://doi.org/10.3390/jmse10020197

Yuan, D., Yin, X., Li, X., Corvianawatie, C., Wang, Z., Li, Y., Yang, Y., Hu, X., Wang, J., Tan, S., Surinati, D., Purwandana, A., Wardana, A.K., Furqon, M., Ismail, A., Budiman, A.S., Bayhaqi, A., Avianto, P., Santoso, P.D., Kusmanto, E., Ari, Z., Pratt, L.J., 2022. A Maluku Sea intermediate western boundary current connecting Pacific Ocean circulation to the Indonesian Through flow. Nat. Commun. 13, 1—8. https://doi.org/10.1038/s41467-022-29617-6

Zhang, X., Wang, H., Wang, S., Liu, Y., Yu, W., Wang, J., Xu, Q., Li, X., 2022. Oceanic internal wave amplitude retrieval from satellite images based on a data-driven transfer learning model. Remote Sens. Environ. 272, 112940. https://doi.org/10.1016/j.rse.2022.112940

Zheng, Q., Klemas, V., Yan, X.-H., Pan, J., 2001a. Nonlinear evolution of ocean internal solitons propagating along an inhomogeneous thermocline. J. Geophys. Res. 106, 14,083—14,094. https://doi.org/10.1029/2000JC000386

Zheng, Q., Yuan, Y., Klemas, V., Yan, X.H., 2001b. Theoretical expression for an ocean internal soliton synthetic aperture radar image and determination of the soliton characteristic half width. J. Geophys. Res. Ocean. 106, 31415—31423. https://doi.org/10.1029/2000jc000726

Zou, P.X., Bricker, J.D., Uijttewaal, W.S.J., 2021. The impacts of internal solitary waves on a submerged floating tunnel. Ocean Eng. 238, 109762. https://doi.org/10.1016/j.oceaneng.2021.109762